Impact of ENSO longitudinal position on teleconnections to the NAO

Article

Accepted Version

Zhang, W., Wang, Z., Stuecker, M. F., Turner, A. G. ORCID: https://orcid.org/0000-0002-0642-6876, Jin, F.-F. and Geng, X. (2019) Impact of ENSO longitudinal position on teleconnections to the NAO. Climate Dynamics, 52 (1-2). pp. 257-274. ISSN 0930-7575 doi: 10.1007/s00382-018-4135-1 Available at https://centaur.reading.ac.uk/70071/

www.reading.ac.uk/centaur

CentAUR

Central Archive at the University of Reading

Reading's research outputs online

Impact of ENSO longitudinal position on teleconnections to the NAO

Wenjun Zhang[1], Ziqi Wang[1], Malte F. Stuecker[2,3], Andrew G. Turner[4,5], Fei-Fei Jin[6], Xin Geng[1]

[1]*CIC-FEMD/ILCEC, Key Laboratory of Meteorological Disaster of Ministry of Education, Nanjing University of Information Science and Technology, Nanjing 210044, China*

[2]*Department of Atmospheric Sciences, University of Washington, Seattle, Washington, USA.*

[3]*Cooperative Programs for the Advancement of Earth System Sciences (CPAESS), University Corporation for Atmospheric Research (UCAR), Boulder, Colorado, USA.*

[4]*NCAS-Climate, University of Reading, Reading RG6 6BB, UK*

[5]*Department of Meteorology, University of Reading, Reading RG6 6BB, UK*

[6]*Department of Atmospheric Sciences, SOEST, University of Hawai'i at Manoa, Honolulu, HI 96822, USA*

Dec. 21, 2017

(*Submitted to Climate Dynamics*)

_____

Corresponding author address:

Dr. Wenjun Zhang

College of Atmospheric Sciences, Nanjing University of Information

Science and Technology, Nanjing 210044, China.

E-mail: zhangwj@nuist.edu.cn

Abstract

While significant improvements have been made in understanding how the El Niño–Southern Oscillation (ENSO) impacts both North American and Asian climate, its relationship with the North Atlantic Oscillation (NAO) remains less clear. Observations indicate that ENSO exhibits a highly complex relationship with the NAO-associated atmospheric circulation. One critical contribution to this ambiguous ENSO/NAO relationship originates from ENSO's diversity in its spatial structure. In general, both eastern (EP) and central Pacific (CP) El Niño events tend to be accompanied by a negative NAO-like atmospheric response. However, for two different types of La Niña the NAO response is almost opposite. Thus, the NAO responses for the CP ENSO are mostly linear, while nonlinear NAO responses dominate for the EP ENSO. These contrasting extra-tropical atmospheric responses are mainly attributed to nonlinear air-sea interactions in the tropical eastern Pacific. The local atmospheric response to the CP ENSO sea surface temperature (SST) anomalies is highly linear since the air-sea action center is located within the Pacific warm pool, characterized by relatively high climatological SSTs. In contrast, the EP ENSO SST anomalies are located in an area of relatively low climatological SSTs in the eastern equatorial Pacific. Here only sufficiently high positive SST anomalies during EP El Niño events are able to overcome the SST threshold for deep convection, while hardly any anomalous convection is associated with EP La Niña SSTs that are below this threshold. This ENSO/NAO relationship has important implications for NAO seasonal prediction and places a higher requirement on models in reproducing

45   the full diversity of ENSO.

1. Introduction

The El Niño–Southern Oscillation (ENSO) is the predominant source of global inter-annual climate variability arising from coupled ocean-atmosphere interactions in the tropical Pacific (Bjerknes 1969; Wyrtki 1975; Schopf and Suarez 1988; Jin 1997; Neelin et al. 1998; Wallace et al. 1998). ENSO has received widespread attention due to its pronounced climate impacts around the globe (e.g., van Loon and Madden 1981; Ropelewski and Halpert 1987, 1996; Trenberth and Caron 2000). For instance, ENSO exhibits impacts on the North American climate via forced atmospheric Rossby waves known as the Pacific-North America (PNA) teleconnection pattern (Hoskins and Karoly 1981; Wallace and Gutzler 1981). Furthermore, ENSO affects East Asian climate through a modulation of the anomalous low-level anticyclone over the western North Pacific (WNP) (e.g., Zhang et al. 1996; Wang et al. 2000). The WNP anomalous anticyclone originates from the nonlinear interactions between ENSO and the warm pool annual cycle (Stuecker et al. 2015; Zhang et al. 2016) and is further amplified by local (Wang et al. 2000; Stuecker et al. 2015) and remote (Yang et al. 2007; Xie et al. 2009, 2016; Stuecker et al. 2015) air-sea coupled processes. In contrast, the linkages between ENSO and climate variability over the North Atlantic-European sector are much less clear.

Interannual variability of North Atlantic-European climate in winter is strongly affected by another prominent atmospheric circulation pattern—the North Atlantic Oscillation (NAO). This pattern represents a large-scale seesaw between the subtropical and polar atmospheric mass. Numerous efforts have been made to explore

68   possible impacts of ENSO on NAO variability since the ENSO/NAO relationship can

69   provide potential seasonal predictability for the climate in Europe (see an extensive

70   review by Brönnimann 2007a). Early research argued that no ENSO-related climate

71   impacts could be identified over the North Atlantic and adjacent Western Europe (e.g.,

72   Rogers 1984; Ropelewski and Halpert 1987; Halpert and Ropelewski 1992). This

73   viewpoint was supported by subsequent studies, indicating that no significant

74   ENSO/NAO connection can be detected (e.g., Trenberth and Caron 2000; Quadrelli et

75   al. 2001; Wang 2002). However, this viewpoint was recently challenged by both

76   observational analyses and various modeling experiments (e.g., Fraedrich and Muller

77   1992; Fraedrich 1994; Dong et al. 2000; Cassou and Terray 2001; Merkel and Latif

78   2002; Moron and Gouirand 2003; Gouirand et al. 2007; Brönnimann et al. 2007b;

79   Ineson and Scaife 2009; Li and Lau 2012a). It is argued that despite large internal

80   variability, a negative NAO-like atmospheric anomaly pattern usually coincides with

81   canonical El Niño events, characterized by a colder and drier-than-normal climate

82   over Western Europe during late winter. Correspondingly, La Niña events display

83   approximately opposite impacts on the NAO.

84   The non-stationary behavior of the ENSO/NAO relationship is possibly

85   associated with different modulating factors, such as natural variability in the

86   extratropical circulation (Kumar and Hoerling 1998), tropical volcanic eruptions

87   (Brönnimannet al. 2007b), other climate signals independent of ENSO (e.g., Mathieu

88   et al. 2004; Garfinkel and Hartman 2010), and decadal changes of the background

89   state (Wu and Zhang 2015). Moreover, the ambiguity of the ENSO/NAO relationship

can be partly attributed to large inter-event variability of both ENSO and the NAO, partly due to short observational records, especially for earlier studies. It is worth mentioning that ENSO's impacts on the NAO are strongly seasonally modulated, with North Atlantic atmospheric anomalies that are approximately opposite in early winter (i.e., November-December) to those in late winter (i.e., January-March) (Moron and Gouirand 2003), which could also lead to discrepancies between different studies.

ENSO exhibits a considerable degree of diversity in its sea surface temperature (SST) anomaly pattern, which also affects its connection with the NAO. In recent decades, a new type of El Niño has been observed frequently in the central Pacific (CP hereafter), which differs considerably from the traditional El Niño that features a SST anomaly center over the Eastern Pacific (EP hereafter) (Larkin and Harrision 2005; Ashok et al. 2007; Weng et al. 2007; Kao and Yu 2009; Kug et al. 2009; Ren and Jin 2011). Many studies have reported the importance in their distinct regional climate impacts (e.g., Weng et al. 2007; Feng et al. 2010; 2016; Feng and Li 2011, 2013; Lee et al. 2010; Zhang et al. 2011, 2013, 2014; Xie et al. 2012; Yu et al. 2012). Similarly, La Niña events can also be separated into two types based on their SST anomaly patterns (Zhang et al. 2015). It is argued that these two ENSO types seem to have different impacts on the NAO (Graf and Zanchettin 2012; Zhang et al. 2015). However, this argument still needs further investigation based on more detailed observational and modeling analyses.

To date, the dynamical mechanisms addressing how tropical SST anomalies associated with ENSO influence the NAO variability have not been fully addressed.

The atmosphere over the North Pacific is usually proposed to serve as the bridge

linking the ENSO-associated diabatic heating in the tropical Pacific with atmospheric

circulation anomalies over the North Atlantic (e.g., Wu and Hsieh 2004; Graf and

Zanchettin 2012). The PNA-like teleconnection pattern over the North Pacific usually

extends downstream to the North Atlantic and leads to a change in the quasi-stationary

wave structures, which can be enhanced by eddy-mean flow interactions (e.g., Cassou

and Terray 2001; Pozo-Vázquez et al. 2005; Graf and Zanchettin 2012). The

stratosphere might also act as a mediator to connect the signal between the Pacific and

Atlantic basins (e.g., Castanheira and Graf 2003; Ineson and Scaife 2009; Bell et al.

2009). As an additional pathway, several previous studies reported that ENSO could

cause northern tropical Atlantic SST anomalies (e.g., Wolter 1987; Curtis and

Hastenrath 1995; Alexander et al. 2002), which then further affect the North Atlantic

atmospheric circulation (e.g., Watanabe and Kimoto 1999; Robertson et al. 2000).

Finally, the ENSO-forced downstream development process of synoptic eddies

provides a pathway to affect the NAO (e.g., Li and Lau 2012a,b; Drouard et al. 2015).

In this argument, the low-frequency atmospheric circulation anomaly (ridge or trough)

over the eastern Pacific and North America is emphasized, which modulates the

meridional propagation of synoptic wave packets over the North Atlantic, which then

favors occurrence of different NAO phases.

As discussed above, there appears little scientific consensus on the ENSO/NAO

relationship and its associated physical mechanisms. For example, can a statistically

significant relationship between ENSO and NAO variability be identified? If so,

134   which dynamical mechanisms are responsible for this relationship? Our previous

135   work provided an evidence for the existence of different types of La Niña based on

136   their different impacts on the NAO (Zhang et al. 2015). The present study extends this

137   analysis and investigates the linear and nonlinear relationships between ENSO and

138   NAO and discusses the dominant mechanisms by using both observations and a suite

139   of numerical model experiments. As we shall demonstrate, predominantly linear and

140   nonlinear NAO responses are found associated with the CP and EP ENSO types,

141   respectively. We will attribute this difference mainly to the varying atmospheric

142   responses to the eastern tropical Pacific SST anomalies.

143   In the reminder of this paper, section 2 introduces the data, methodology,

144   definition of ENSO events, and our experimental design. Section 3 illustrates

145   uncertainties of the ENSO/NAO relationship. The different linkages between the

146   NAO and the two distinct ENSO types are examined in section 4. Further evidence of

147   this complex ENSO/NAO relationship is shown in section 5. Possible dynamical

148   mechanisms for the different ENSO/NAO relationships are discussed in section 6. The

149   major conclusions are summarized and discussed in section 7.

150

151 **2. Data, Methodology, definition of ENSO events, and Experimental**

152 **design**

153 **2.1 Data and Methodology**

154   Monthly SST anomalies associated with ENSO were examined based on the

155   Hadley Centre sea ice and SST data set (HadISST) version 1.1 (Rayner et al. 2003).

156   The atmospheric circulation was investigated using National Center for

157   Environmental Prediction (NCEP)/National Center for Atmospheric Research (NCAR)

158   reanalysis-1 data (Kalnay et al. 1996). Precipitation data are taken from the Global

159   Precipitation Climatology Centre (GPCC) (Rudolf et al. 2005). We also utilized the

160   global monthly land surface temperature analysis collected from the Global Historical

161   Climatology Network version 2 and the Climate Anomaly Monitoring System

162   (GHCN_CAMS) (Fan and van den Dool 2008). To describe the NAO-associated

163   atmospheric activity, the NAO index is defined as the difference in normalized

164   sea-level pressure (SLP) zonally-averaged from 80°W to 30°E between 35°N and

165   65°N (Li and Wang 2003). Other NAO indices, such as the index defined by Hurrell

166   (Hurrell   1995)   and   Climate   Prediction   Center   (CPC;

167   http://www.cpc.ncep.noaa.gov/products/precip/CWlink/pna/nao.shtml)   were   also

168   examined and the conclusions remain the same.

169   Our analyses in this paper cover the period 1948-2014 and anomalies for all

170   variables were computed as the deviations from a 30-year climatological mean

171   (1981–2010). A 6-120 month band-pass filter was applied to each dataset using the

172   second-order Butterworth filter designed by Parks and Burrus (1987), to focus on

173   ENSO-related interannual variability. The first and last three years of the datasets

174   were removed in the following analyses to avoid possible boundary distortion

175   associated with the band-pass filtering. Linear correlation and composition analyses

176   were used to investigate the ENSO/NAO relationship. Statistical significance was

177   determined using the two-tailed Student's t-test.

2.2 Definition of ENSO events

ENSO events usually reach their peak phase during boreal winter (December-January-February, DJF). However, the largest impact of ENSO on the NAO can usually be found during late winter (January-February-March, JFM) (e.g., Zhang et al. 2015). Thus, we use the DJF Niño3.4 index (SST anomalies averaged over 5°S–5°N and 120°–170°W) as a measure of ENSO and the NAO index calculated in JFM to characterize the NAO. The CPC definition is utilized to identify ENSO winters based on a threshold of ± 0.5℃ of the Niño3.4 SST anomalies for five consecutive overlapping seasons. Many regional ENSO indices are able to separate El Niño events into two types (i.e., Ashok et al. 2007; Kao and Yu 2009; Ren and Jin 2011), however they fail to effectively distinguish different La Niña types (Zhang et al. 2015), especially during the period before the 1980s (Ren et al. 2013). Here we identify different ENSO types by the spatial distribution of SST anomalies, same as our previous definition (Zhang et al. 2011, 2013, 2014, 2015), which can effectively distinguish two types for both El Niño and La Niña events. The events are classified into EP (CP) ENSO winters if the largest SST anomaly center occurs east (west) of 150°W during the developing and mature (September to February) ENSO phases. Among them, two El Niño events (1987/88, 2006/07) and three La Niña events (1970/71, 1999/00, 2007/08) are defined as a mixed type (or basin-wide mode) since the SST anomalies cover both EP and CP regions. Here, ENSO years are labeled Year(0)/Year(1), where 0 and 1 refer to the ENSO developing and decaying year, respectively. Some ENSO events coincide with tropical volcanic eruptions, which

10

200   strongly affect the atmospheric circulation over the North Atlantic and Europe for

201   about 1-2 years after the eruption (e.g., Robock 2000; Driscoll et al. 2012). Hence,

202   ENSO events (i.e., 1982/83 and 1991/92) following major tropical volcanic eruptions

203   are excluded in our analysis. Especially for the 1991 Pinatubo eruption, the second

204   largest eruption in the 20th century, its climate impacts over Europe can be detected

205   after several years following the eruption (e.g., Xiao and Li 2011). To exclude these

206   volcanic eruption signals, the following two and four years were removed after the

207   1982 and 1991 eruptions, respectively. The two types of ENSO winters analyzed in

208   this paper are listed in Table 1. Each category features 8 samples, other than the CP

209   El Niño group, which contains 9 events.

210

211   **2.3 Experimental design**

212   To examine the possible impacts of ENSO SST anomalies on the NAO, modeling

213   experiments were conducted using the Geophysical Fluid Dynamics Laboratory

214   (GFDL) global Atmospheric Model version 2.1 (AM2.1) (The GFDL Global

215   Atmospheric Model Development Team, 2004) with a horizontal resolution of 2.5°

216   longitude×2° latitude. As a reference state, climatological (seasonally varying) SSTs

217   were used to force the atmospheric model. Additionally, a suite of sensitivity

218   experiments (EPW, CPW, EPC, and CPC) was designed (Table 2). For the first

219   simulation (EPW), the SST anomalies for composites of the EP El Niño events listed

220   in Table 1 were imposed on the monthly climatological SST from October to February

221   in the tropical Pacific (30°S-30°N, 120°E-90°W) (Table 2). Anomalies outside of the

11

222 region were set to zero to limit our analysis to the effects of tropical Pacific SST

223 anomalies. We note that the SST anomalies outside of the tropical Pacific also play

224 some role in ENSO-induced climate impacts, which are not considered in this paper.

225 The other three experiments (CPW, EPC, and CPC in Table 2) are the same as the

226 EPW experiment, except that the SST anomalies are the composites for other different

227 ENSO types (the CP El Niño, EP La Niña, and CP La Niña events in Table 1). Each

228 simulation is integrated for 15 years and the last 10 years of the integrations were used

229 to avoid influences of the initial conditions. A composite of these 10 years removes

230 most of the internal variability.

231

3. Uncertainties of the ENSO/NAO relationship

233 First, we investigate the time series of the DJF Niño3.4 and JFM NAO indices

234 (Fig. 1a). These two indices display conspicuous interannual variability that is only

235 weakly anti-correlated (R=-0.23, insignificant at the 95% confidence level). Also, no

236 robust linear relationship can be established when considering sliding correlations

237 with 11- and 21-year windows respectively (Fig. 1b). To address possible influences

238 of volcanic eruption events on the ENSO/NAO relationship, we further calculate the

239 correlation coefficient between the Niño3.4 and NAO indices after removing the

240 previously defined eruption years from both time series. After removing this influence,

241 we detect a weak but statistically significant (at the 95% confidence level)

242 relationship (R=-0.33 in Table 3), suggesting that in general El Niño events (as

243 measured by DJF Niño3.4) tend to be accompanied by a negative NAO phase, and La

244   Niña events by a positive NAO.

245   Next, we show a scatterplot of Niño3.4 and NAO indices during the ENSO

246   winters (Fig. 2). Most (14 of 17) El Niño events are accompanied by a negative NAO

247   phase, consistent with many previous studies (e.g., Brönnimann 2007a; Li and Lau

248   2012a). Only three El Niño events (i.e., 1953/54, 1972/73, 2002/03) coincide with a

249   weak positive NAO phase. However, no simple relationship is detected between the

250   Niño3.4 and NAO indices for La Niña events. Around half of the La Niña winters

251   exhibit a positive NAO phase, while the other half are accompanied by a negative

252   NAO phase. We hypothesize that this unstable La Niña/NAO relationship could

253   explain the weak correlation between the Niño3.4 and NAO indices. To better

254   understand the different NAO response to La Niña, we show the composite SST

255   anomaly patterns during La Niña/NAO+ (Fig. 3a) and La Niña/NAO- (Fig. 3b)

256   winters. La Niña winters corresponding to a positive NAO phase exhibit a negative

257   SST anomaly center, strongest over the central equatorial Pacific west of 150°W with

258   relatively weak anomalies in the eastern equatorial Pacific, which is the characteristic

259   pattern of the CP La Niña (Zhang et al. 2015). In contrast, the SST anomalies

260   associated with La Niña/NAO- events have maximum negative SST anomalies in the

261   equatorial eastern Pacific east of 150°W, which resembles the SST anomaly pattern of

262   the EP La Niña. This suggests that the NAO responses are very sensitive to the zonal

263   location of La Niña-related SST anomalies, which have been described in our

264   previous study (Zhang et al. 2015). This separation of La Niña events with regard to

265   NAO phase is also evident in Figure 2. This suggests that ENSO has indeed a close

266 connection with the NAO, which was not easily detected in earlier studies due to the

267 nonlinear La Niña/NAO relationship.

268

4. Inconsistent linkages between the NAO and two types of ENSO

270 Next, we investigate ENSO event composites to further examine the relationship

271 between the NAO and the two types of ENSO. First, we show the SST anomaly

272 patterns to demonstrate the validity of two-type ENSO classification (Fig. 4). It can be

273 seen that the SST anomaly patterns related to the different ENSO types are well

274 separated. They are characterized by a different zonal location of the SST anomalies

275 and the corresponding near-surface wind anomalies (SST maxima at approximately

276 165°W and 115°W for CP and EP ENSO respectively). Note that the SST anomaly

277 patterns associated with the two La Niña types are almost the same as those shown in

278 Figure 3 associated with different phases of the NAO. Furthermore, it can be seen that

279 the SST amplitude is larger for EP El Niño than for CP El Niño. In contrast, the SST

280 amplitude for EP La Niña is smaller than for CP La Niña.

281 To examine the extra-tropical response, Northern Hemisphere composite SLP

282 anomalies for the different ENSO types are shown in Figure 5. We observe an

283 atmospheric Rossby wave response to diabatic heating caused by positive SST

284 anomalies in the tropical Pacific. Positive PNA-like atmospheric circulation patterns

285 are seen during both EP and CP El Niño winters, albeit with different spatial extent

286 and amplitude (Fig. 5a, b). Compared to the EP El Niño composite, we observe

287 negative SLP anomalies over the North Pacific for CP El Niño that are shifted

288   southeastward and have a larger extent. Importantly, both EP and CP El Niño winters

289   exhibit extra-tropical atmospheric responses of the same sign over the Atlantic. In

290   comparison, the negative NAO-like SLP response (characterized by weakened

291   subtropical high and polar low) is larger for CP than EP El Niño events, despite the

292   larger SST amplitude during EP El Niño events. Unlike the CP El Niño events, the EP

293   El Niño-associated SLP anomalies over the North Atlantic are relatively weak and are

294   significant only above the 80% confidence level, thus exhibiting a certain degree of

295   uncertainty. This uncertainty could be due to the large diversity in the amplitude of EP

296   El Niño events (Toniazzo and Scaife 2006). Differences in teleconnection patterns

297   associated with the two El Niño types can also be observed in the Southern

298   Hemisphere (Lim et al., 2013; Wilson et al., 2014, 2016). In the Northern Hemisphere,

299   both La Niña types are characterized by negative PNA-like atmospheric circulation

300   anomalies that appear as a response to the negative SST anomalies in the tropical

301   Pacific (Fig. 5c,d). Correspondingly, positive SLP anomalies are evident for both

302   types over the North Pacific, indicating a weakened Aleutian low. In contrast, the CP

303   La Niña-associated SLP anomalies are displaced southeastward compared to the EP

304   La Niña, which is similar to the Pacific signal seen for the two El Niño types. Despite

305   these similar anomalies over the North Pacific, an almost opposite atmospheric

306   anomaly is observed over the North Atlantic and Western Europe for the two La Niña

307   types. The EP La Niña events exhibit a negative NAO-like atmospheric response

308   (weakened subtropical high and polar low) with its center located over the eastern

309   North Atlantic and Western Europe (Fig. 5c). In contrast, the CP La Niña events are

310 accompanied by a positive NAO-like atmospheric anomaly pattern (strengthened

311 subtropical high and polar low) with its center located over the western-to-central

312 North Atlantic (Fig. 5d). These NAO-like responses to different ENSO types can in

313 fact be seen for almost the entire troposphere over the North Atlantic (Fig. 6),

314 exhibiting a quasi-barotropic structure. Notably, the North Atlantic response seems

315 weak for mid-latitude negative anomalies during EP El Niño events (Fig.6a).

316   The subtropical jet is usually argued to serve as a mediator linking ENSO and the

317 North Atlantic atmosphere (e.g., Graf and Zanchettin 2012). Figure 7 shows the

318 composite 300 hPa zonal wind anomalies during different types of ENSO winters. For

319 both types of El Niño events, the zonal wind anomalies exhibit a tripolar structure and

320 tilt slightly northeastward (Fig. 7a,b). These anomalies extend zonally from the North

321 Pacific toward the North Atlantic. Similar to Figure 5a, the EP El Niño-associated

322 anomalies are relatively weak over the North Atlantic and statistically significant only

323 above the 80% confidence level. In contrast, the CP El Niño-associated anomalies

324 exhibit a larger zonal extent and amplitude than those for EP El Niño. Overall, the

325 Atlantic subtropical westerly jet tends to be weakened for both El Niño types,

326 corresponding to the negative NAO-like atmospheric responses. A very similar

327 meridional structure of 300 hPa zonal wind anomalies is observed for the two La Niña

328 types over the North Pacific, but with farther northward displacement by about 10° for

329 EP La Niña compared to CP La Niña (Fig. 7c,d). The CP La Niña-related zonal wind

330 anomalies extend to the North Atlantic and Western Europe region, where

331 anomalously weak upper-level winds are found as far east as the Mediterranean. In

332 contrast, the EP La Niña-associated zonal wind anomalies are more zonally

333 constrained (more like a wave train structure) and of almost opposite structure over

334 the North Atlantic. Consistent with the NAO response, a weakened and strengthened

335 Atlantic jet concurs with EP and CP La Niña events, respectively (Fig. 7c,d).

336 Interestingly, the 300 hPa wind response to CP ENSO is quite linear, with roughly

337 equal and opposite patterns in response to CP El Niño and CP La Niña (Fig. 7b,d).

338 This is not the case for EP ENSO where the response is distinctly nonlinear.

339 Corresponding to the different Atlantic jet anomalies, the activity of the synoptic

340 eddies (2-10-day timescale) is weakened over the North Atlantic for the two El Niño

341 types and EP La Niña events, while it is strengthened for CP La Niña events (not

342 shown). Again, the eddy response to ENSO forcing from the CP region is quite linear,

343 while it is nonlinear for EP ENSO.

344

345 **5. Observed and simulated evidence for a complex ENSO/NAO**

346 **relationship**

347 5.1 Observed surface temperature anomalies associated with different ENSO types

348 We use the observed surface temperature data to further investigate the identified

349 complex ENSO/NAO relationship. Previous studies have pointed out that the

350 anomalous surface climate conditions (such as temperature) over Western Europe and

351 even Eurasia are closely associated with NAO phase (for a review, refer to Jones et al.

352 2003). Motivated by our previous analyses we hypothesize that different ENSO types

353 may give rise to distinct climate anomalies over Eurasia. As shown in Section 4, the

17

354   negative NAO-like responses to the two El Niño types and EP La Niña events are

355   accompanied by a weakened Atlantic jet (Fig. 7a-c), which limits the transport of

356   warm and moist air from the North Atlantic to the northern Eurasian land areas.

357   Simultaneously, the strengthened zonal winds south of the Atlantic jet core (Fig. 7a-c)

358   lead to enhanced warm and moist air transported into southern Eurasia. As expected,

359   northern Eurasia (roughly north of 40°N) experiences a colder than normal winter

360   during the two types of El Niño and EP La Niña (Fig. 8a-c). At the same time, the

361   southern part of Eurasia tends to experience warmer than normal winters. In contrast,

362   CP La Niña events tend to result in positive NAO-like atmospheric anomalies and a

363   strengthened Atlantic jet. Therefore, warmer and wetter air can be transported into

364   northern Eurasia, which results in positive surface temperature anomalies in Europe

365   during CP La Niña winters (Fig. 8d). Precipitation anomaly differences are

366   approximately co-located with the surface temperature anomalies, characterized by

367   reduced precipitation for the two El Niño types and EP La Niña and enhanced

368   precipitation for CP La Niña over northern Eurasia (not shown), albeit with much

369   larger spatial non-uniformity. Although EP and CP El Niño events have similar

370   impacts on the Eurasian climate, a remarkable difference is evident in the spatial

371   extent and amplitude of the climate anomalies (Fig. 5 and 8).

372

373   5.2 Experiments of ENSO forcing on European climate variability

374   We utilize a series of general circulation model experiments to verify the

375   identified NAO impacts of tropical SST anomalies associated with different ENSO

18

376 types (as listed in Table 2 and described in Section 2.3). Figure 9 shows the

377 anomalous sea-level pressure (SLP) responses to the different prescribed ENSO

378 forcings. Simulated EP and CP El Niño winters are both characterized by a

379 strengthened Aleutian Low and negative NAO phase (Fig. 9a,b), which is roughly

380 consistent with the observations. Both EP and CP La Niña forcings generate a

381 weakened Aleutian Low. However, they simulate almost opposite atmospheric

382 responses over the North Atlantic (Fig. 9c,d), which can also be seen in experiments

383 conducted with the NCAR Community Atmospheric Model version 5 (CAM5; Zhang

384 et al. 2015). Consistent with observations, opposite NAO responses are found when

385 the EP and CP La Niña-related SST anomalies are imposed. It is notable that the

386 simulated atmospheric responses over Western Europe are weaker than what we see in

387 the observations (Figure 5c and 9c).

388 We further inspect the subtropical jet anomalies in these experiments, since it

389 plays an important role in connecting the ENSO signal with the North Atlantic

390 atmosphere. Figure 10 displays the simulated 300 hPa zonal wind anomalies during

391 winter for different ENSO types. Consistent with the observations (Fig. 7a,b), the

392 simulated zonal wind anomalies exhibit a tripolar structure over the North Pacific and

393 extend zonally from there toward the North Atlantic for both types of El Niño events.

394 The weakened Atlantic jet is also well reproduced in these experiments. Moreover,

395 almost opposite 300 hPa wind responses are well reproduced in the CP La Niña

396 experiments. Also consistent with the observations, the simulated zonal wind

397 anomalies are mostly confined west of 60°W with an opposite structure over the

398   North Atlantic for the EP La Niña compared to CP La Niña events. The fact that these

399   features are simulated in our idealized experiments suggests that the different NAO

400   responses to EP and CP ENSO may be robust. We note that some obvious differences

401   exist in the EP El Niño composites between the observations and the model

402   simulation, but importantly they both consistently capture the positive PNA phase and

403   negative NAO phase. These differences could be partly explained by the large

404   inter-event variability in amplitude of EP El Niño events. In particular, the super El

405   Niño events (e.g., 1972/73 and 1997/98) display pronounced differences in local

406   air-sea coupled features and in the SST anomalies outside of the tropical Pacific

407   region, which are not considered in our experimental design.

408

409   **6. Possible mechanisms for the unstable ENSO/NAO relationship**

410   Our analyses so far demonstrated that different ENSO types exhibit complex

411   linkages with the NAO phase. CP ENSO (i.e., CP El Niño and CP La Niña) displays

412   linear impacts on the NAO. In contrast, EP ENSO (i.e., EP El Niño and EP La Niña)

413   shows nonlinear impacts on the NAO. To explore possible reasons for these

414   differences, we decompose analysis into linear and nonlinear SST and atmospheric

415   anomalies associated with the two ENSO types (Fig. 11). The degree of nonlinearity is

416   determined by adding composites from two opposing phases of ENSO. Should the

417   result be zero (i.e., the patterns associated with a particular field are exactly equal and

418   opposite for El Niño and La Niña phases), then the ENSO response is perfectly linear.

419   Precipitation associated with tropical deep convection is a good indicator of the

420   linearity of the impacts of tropical SST anomalies, with the caveat that precipitation

421   observations over the ocean are only available after the late 1970s. Thus, we use SLP

422   anomalies to explore the local atmospheric response over the tropical Pacific instead

423   of precipitation. Positive SST and negative SLP anomalies are evident in the eastern

424   tropical Pacific, while negative SST and positive SLP anomalies exist in the western

425   tropical Pacific for the linear part of EP ENSO (Fig. 11a), thus displaying typical EP

426   ENSO features. In contrast, the linear SST anomalies for the CP ENSO are shifted

427   westward to the central and western tropical Pacific (Fig. 11b). Correspondingly, the

428   linear part of negative SLP anomalies exhibits the same westward shift for CP ENSO

429   events. Importantly, CP ENSO does not exhibit a significant nonlinear component

430   over the equatorial Pacific (Fig. 11d is mostly near-zero). This implies that negative

431   and positive CP ENSO events will also not excite nonlinear teleconnection anomalies

432   over the extra-tropics. Although almost no nonlinear SST anomaly appears over the

433   tropical Pacific for the EP ENSO, we observe a strong nonlinear SLP anomaly

434   response to the EP ENSO (Fig. 11c), whose amplitude is comparable to the linear

435   component (compared to Fig. 11a).

436   Next, we examine the experimental results to verify the different relationships

437   between SST forcing and atmospheric responses for these two ENSO types. For the

438   linear part, the observed SLP features are well captured by the experiments forced

439   with EP ENSO-related SSTs in the tropical Pacific. For example, positive and

440   negative SLP anomalies emerge over the western and eastern tropical Pacific,

441   respectively (Fig. 12a). Similarly, the tropical Pacific SST forcing associated with CP

442   ENSO can reproduce the westward extension of the SLP response compared to EP

443   ENSO (Fig. 12b). In comparison, relatively large negative SLP anomalies are seen in

444   the eastern tropical Pacific for the EP nonlinear component (Fig. 12c), which cannot

445   be seen for the CP case (Fig. 12d). Consistent with the observations, the atmospheric

446   responses to the two types of ENSO are very different over the eastern tropical Pacific,

447   despite a systematic bias in the northern and western tropical Pacific for both EP and

448   CP ENSO events. These biases are possibly attributed to a combination of the

449   idealized experimental design (SST anomalies are set to zero outside of the tropical

450   Pacific), a one-way forcing from the ocean to atmosphere without considering

451   coupled ocean-atmosphere feedbacks, and model mean state biases.

452   Tropical convection depends critically on the total SST (climatology plus

453   anomalies), thus convection and associated SLP anomalies usually exhibit a nonlinear

454   relationship with SST anomalies. As the CP region is located near the eastern edge of

455   the tropical Pacific warm pool with relatively high climatological SSTs, anomalous

456   convection exhibits a quasi-linear relationship with SST anomalies. In contrast, the

457   climatological SSTs are well below the SST threshold for convection in the EP region.

458   Therefore, negative SST anomalies have only a small impact on local convection,

459   while positive SST anomalies associated with EP El Niño events can lead to strong

460   local convention and precipitation anomalies.

461   The linear and nonlinear components of the simulated precipitation are shown in

462   Fig. 13 to confirm the greater nonlinear atmospheric responses to ENSO in the eastern

463   tropical Pacific. The composite difference between positive and negative phases of

464   ENSO (the linear response) shows positive precipitation anomalies in the eastern

465   equatorial Pacific (155°-90°W, 5°S-5°N) for both EP and CP ENSO (the latter of

466   approximately half amplitude compared to EP ENSO). For the simulated nonlinear

467   component, positive precipitation anomalies are evident in the eastern Pacific for the

468   EP ENSO forcing (indicating a high degree of nonlinearity), with amplitude

469   comparable to the CP linear component. In contrast, almost no nonlinear precipitation

470   anomalies are seen for the CP ENSO forcing. The degree of nonlinearity could also be

471   diagnosed as the ratio of the magnitudes of nonlinear to linear components.

472   Hence, the nonlinear relationship between SST and atmospheric response can be

473   well reproduced by the model experiments. We emphasize that these nonlinear

474   convection anomaly responses result in very different teleconnection patterns over the

475   extra-tropics. Therefore, this nonlinearity is likely an important factor for determining

476   the distinct NAO responses to different ENSO types in the observation.

477

478   7. Conclusions and Discussion

479   We use reanalysis data in conjunction with ENSO and NAO indices of the

480   1948-2014 period to determine impacts of different ENSO types (central and east

481   Pacific events, CP and EP) on North Atlantic climate variability. A stable

482   relationship is found between ENSO and atmospheric anomalies in the North Pacific

483   region. However, no consistent linear relationship is found between ENSO and the

484   NAO. We found that the complex ENSO/NAO relationship is mainly modulated by

485   the different ENSO flavors once the impacts of volcanic activity are removed. Both

486   types of El Niño (EP and CP) are accompanied by a negative NAO phase over the

487   North Atlantic, albeit with different intensities. In contrast, almost opposite

488   atmospheric anomaly structures are detected over the North Atlantic for the two

489   types of La Niña. A positive NAO phase is associated with CP La Niña winters,

490   while a negative NAO phase is associated with the EP La Niña winters. Moreover,

491   these results based on the reanalysis data are evidenced by the observed land surface

492   temperature over the Eurasian region and reproduced by the experiments driven by

493   imposed tropical Pacific SST anomalies associated with ENSO. We note that the

494   composite NAO-associated atmospheric anomalies for EP ENSO events, especially

495   for EP El Niño, are weaker than those to CP ENSO events. This difference may be

496   due to different zonal locations of the ENSO-related air-sea action center. Compared

497   to CP ENSO events, the EP ENSO-associated SST anomalies are located in the

498   eastern tropical Pacific where the climatological SSTs are colder. These different

499   background states likely explain why the atmospheric responses to the same SST

500   anomaly amplitude are weaker. In addition, the large diversity among amplitude of

501   EP El Niño events increases the uncertainty in their climate impacts.

502   While CP ENSO events display linear impacts on the North Atlantic

503   atmospheric circulation, EP ENSO events exhibit nonlinear impacts. These varying

504   extra-tropical atmospheric responses to two different ENSO types are mainly related

505   to local nonlinear air-sea coupling in the tropical Pacific. Although the SST

506   anomalies for our ENSO type composites are quasi-linear, we observe very different

507   local atmospheric responses due to the nonlinear SST threshold for deep convection.

24

508   Thus, our conclusion is that nonlinear local atmospheric responses can further lead to

509   different extra-tropical atmospheric anomalies (such as the NAO) since they will

510   excite different wave propagation patterns through the troposphere.

511   Although ENSO originates in the tropical Pacific, its impacts can be detected in

512   remote oceans through the so-called atmospheric bridge mechanism (e.g., Klein et al.

513   1999; Alexander et al. 2002). Some studies reported that ENSO-associated tropical

514   Atlantic SST anomalies could serve as a mediator to connect the tropical Pacific SST

515   anomalies with the NAO (e.g., Watanabe and Kimoto 1999; Robertson et al. 2000). As

516   seen previously (Fig. 4a,b), pronounced positive SST anomalies are evident in the

517   northwestern tropical Atlantic during EP Niño events, which are absent during CP El

518   Niño events. In contrast, negative SST anomalies occur in the northern tropical

519   Atlantic for both EP and CP La Niña events (Fig. 4c,d). Our experiments show that

520   only tropical Pacific SST anomaly forcings associated with different ENSO types can

521   well reproduce the observed NAO responses, suggesting that tropical Atlantic SST

522   anomalies are not a key factor for the NAO responses to ENSO. Moreover, our

523   previous experiments suggested that these tropical Atlantic SST anomalies during

524   ENSO events could play a minor role for the NAO (Zhang et al. 2015). To further

525   investigate possible effects of tropical Atlantic SST anomalies on the extra-tropical

526   atmospheric circulation, we show in Fig. 14 the partial correlation coefficient of the

527   observed SLP anomalies with SST anomalies in the tropical North Atlantic (0°–30°N,

528   20°–80°W), after the ENSO influence was linearly removed. Pronounced positive and

529   negative SLP anomalies emerge over the north and south of the North Atlantic

530   respectively, a pattern that resembles a negative NAO phase. However, no significant

531   Aleutian Low anomalies can be found over the Pacific basin. This indicates that SST

532   anomalies in the tropical North Atlantic could have some contribution to the NAO

533   although they are not able to induce large-scale extra-tropical atmospheric circulation

534   anomalies in the same way as ENSO. However, SST anomalies in the tropical North

535   Atlantic seem unable to explain diverging NAO responses to different ENSO types.

536   A scientific question that remains unresolved is how the tropical Pacific SST

537   anomalies associated with different ENSO types result in varying NAO responses. To

538   explore possible effects of stratospheric processes, we inspected the signal of the

539   zonal wind anomalies at 60°N (Fig. 15) and found no significant signal propagation

540   from the stratosphere to troposphere. This result is supported by our model

541   experiments (not shown). However, we cannot fully exclude the possibility that the

542   stratosphere plays a role in the ENSO/NAO connection due to sparse input

543   observations to the reanalysis assimilation scheme, and poor performance of the

544   model at upper levels. For example, a recent study argued that ENSO have impacts on

545   climate over Northern Atlantic and Eurasia mainly through the stratospheric pathway

546   (Butler et al. 2014).

547   Another possible cause of the divergent NAO responses to different ENSO types

548   could be the downstream development of synoptic eddies. The low-frequency

549   atmospheric anomalies over the northeast Pacific are very important for the

550   propagation of the Pacific jet (Drouard et al. 2015). For example, the ridge anomaly

551   over the northeastern Pacific can deflect the Pacific jet while the trough anomaly in

552 this location can maintain the Pacific jet extending in a zonal orientation. Therefore,

553 during both types of El Niño events the trough anomaly over the northeastern Pacific

554 favors a zonally oriented propagation of the Pacific jet. In contrast, the zonal location

555 of the Northern Pacific SLP anomalies for both La Niña types differs significantly

556 (Figure 5c,d). During CP La Niña, high SLP anomalies are shifted southward

557 (compared to EP La Niña) and the northeastern Pacific is characterized by weak

558 negative SLP anomalies. Thus, the Pacific jet extends zonally from the Pacific to the

559 North Atlantic. For the EP La Niña, high SLP anomalies are located over the

560 northeast Pacific, which act to deflect the Pacific jet. According to the study by

561 Drouard et al. (2015), the different propagation orientation of the Pacific jet could

562 result in varying downstream eddy structures and thus cause opposite NAO phases.

563   This paper adds to the body of work stating the importance of taking ENSO

564 diversity into account when considering its impacts on remote climate variability.

565 Coupled dynamical seasonal prediction models in use at various meteorological

566 agencies must therefore be able to simulate the range of ENSO diversity in terms of

567 its longitudinal location in order to correctly capture any additional skill offered to the

568 NAO.

569

578

Reference

Ashok K, Behera SK, Rao SA, Weng HY, Yamagata T (2007) El Niño Modoki and its possible teleconnection. J Geophys Res 112:C11007. doi:10.1029/2006JC003798

Alexander MA, Bladé I, Newman M, Lanzante JR, Lau NC, Scott JD (2002) The atmospheric bridge: The influence of ENSO teleconnections on air–sea interaction over the global oceans. J Clim 15:2205–2231

Bell CJ, Gray LJ, Charlton-Perez AJ, Joshi MM (2009) Stratospheric communication of El Niño teleconnections to European winter. J Clim 22:4083–4096

Bjerknes J (1969) Atmospheric teleconnections from the equatorial Pacific. Mon Wea Rev 97:163–172

Brönnimann S (2007a) Impact of El Niño–Southern Oscillation on European climate. Rev. Geophys 45:RG3003. doi:10.1029/2006RG000199

Brönnimann S, Xoplaki E, Casty C, Pauling A, Luterbacher J (2007b) ENSO influence on Europe during the last centuries. Clim Dyn 28:181–197

Butler AH, Polvani LM, Deser C (2014) Separating the stratospheric and tropospheric pathways of El Niño–Southern Oscillation teleconnections. Environ Res Lett 9: 024014. doi:10.1088/1748-9326/9/2/024014

Cassou C, Terray L (2001) Oceanic forcing of the wintertime low-frequency atmospheric variability in the North Atlantic European sector: A study with the ARPEGE model. J Clim 14: 4266–4291

Castanheira JM, Graf HF (2003) North Pacific–North Atlantic relationships under stratospheric control? J Geophys Res 108:4036. doi:10.1029/2002JD002754

Curtis S, Hastenrath S (1995) Forcing of anomalous sea-surface temperature evolution in the tropical Atlantic during Pacific warm events. J Geophys Res 100C: 15835–15847.

Dong BW, Sutto RT, Jewson SP, O'Neill A, Slingo JM (2000) Predictable winter climate in the North Atlantic sector during the 1997–1999 ENSO cycle. Geophys Res Lett 27:985–988

Driscoll S, Bozzo A, Gray LG, Robock A, Stenchikov G (2012) Coupled Model

608   Intercomparison Project 5 (CMIP5) simulations of climate following volcanic

609   eruptions. J Geophys Res 117:127-135

610 Drouard M, Riviere G, Arbogast P (2015) The link between the North Pacific climate

611   variability and the North Atlantic Oscillation via downstream propagation of

612   synoptic waves. J Clim 28:3957–3976

613 Fan Y, van den Dool H (2008) A global monthly land surface air temperature analysis

614   for 1948-present. J Geophys Res 113:D01103. doi:10.1029/2007JD008470

615 Feng J, Li JP (2011) Influence of El Niño Modoki on spring rainfall over South China.

616   J Geophys Res 116:D13102. doi:10.1029/2010JD015160

617 Feng J, Li JP (2013) Contrasting impacts of two types of ENSO on the boreal spring

618   Hadley circulation. J Clim 26:4773-4789

619 Feng J, Li JP, Zheng F, Xie F, Sun C (2016) Contrasting impacts of developing phases

620   of two types of El Niño on southern China rainfall. J. Meteor. Soc. Japan, 94,

621   359–370

622 Feng J, Wang L, Chen W, Fong SK, Leong KC (2010) Different impacts of two types

623   of Pacific Ocean warming on Southeast Asia rainfall during boreal winter. J

624   Geophys Res 115:D24122. doi:10.1029/2010JC014761

625 Fraedrich K (1994) ENSO impact on Europe?—A review. Tellus Ser A 46:541–552

626 Fraedrich K, Muller K (1992) Climate anomalies in Europe associated with ENSO

627   extremes. Int J Climatol 12:25–31

628 Garfinkel CI, Hartmann DL (2010) Influence of the quasi-biennial oscillation on the

629   North Pacific and El Niño teleconnections. J Geophys Res 115:D20116.

630   doi:10.1029/2010JD014181

631 Graf HF, Zanchettin D (2012) Central Pacific El Niño, the ''subtropical bridge'', and

632   Eurasian climate. J Geophys Res 117:D01102

633 Gouirand I, Moron V (2003) Variability of the impact of El Niño–Southern

634   Oscillation on sea-level pressure anomalies over the North Atlantic in January to

635   March (1874–1996). Int J Climatol 23:1549–1566

636 Halpert MS, Ropelewski CF (1992) Surface temperature patterns associated with the

637   Southern Oscillation. J Clim 5:577–593

638   Hoskins BJ, Karoly DJ (1981) The steady linear response of a spherical atmosphere to

639   thermal and orographic forcing. J Atmos Sci 38:1179–1196

640   Huang RH, Wu YF (1989) The influence of ENSO on the summer climate change in

641   China and its mechanism. Adv Atmos Sci 6:21–32

642   Hurrell JW (1995) Decadal Trends in the North Atlantic Oscillation: Regional

643   Temperatures and Precipitation. Science 269:676-679

644   Ineson S, Scaife AA (2009), The role of the stratosphere in the European climate

645   response to El Niño. Nature Geoscience 2:32–36

646   Jin FF (1997) An equatorial ocean recharge paradigm for ENSO. Part I: Conceptual

647   model. J Atmos Sci 54:811–829

648   Jin FF, An SI, Timmermann A, Zhao J (2003) Strong El Niño events and nonlinear

649   dynamical heating. Geophys Res Lett 30:1120. doi: 10.1029/2002GL016356

650   Jones PD, Osborn TJ, Briffa KR (2003) Pressure-based measurements of the North

651   Atlantic Oscillation (NAO): A comparison and an assessment of changes in the

652   strength of the NAO and in its influence on surface climate parameters. AGU

653   Geophys Monogr 34:51-62

654   Kalnay E, Coauthors (1996) The NCEP/NCAR 40-Year Reanalysis Project. Bull

655   Amer Meteor Soc 77:437–471

656   Kao HY, Yu JY (2009) Contrasting eastern-Pacific and central-Pacific types of ENSO.

657   J Clim 22:615–632

658   Klein SA, Soden BJ, Lau NC (1999) Remote sea surface temperature variations

659   during ENSO: Evidence for a tropical atmospheric bridge. J Clim 12:917–932

660   Kug JS, Jin FF, An SI (2009) Two types of El Niño events: Cold tongue El Niño and

661   warm pool ElNiño. J Clim 22:1499–1515

662   Kumar A, Hoerling MP (1998) Annual cycle of Pacific/North American seasonal

663   predictability associated with different phases of ENSO. J Clim 11:3295–3308

664   Larkin NK, Harrison DE (2005) On the definition of El Niño and associated seasonal

665   average U.S. weather anomalies. Geophys Res Lett 32:L13705.

666   doi:10.1029/2005GL022738

667   Lee SK, Wang C, Enfield DB (2010) On the impact of central Pacific warming event

668   on Atlantic tropical storm activity. Geophys. Res. Lett., 37, L17702,

669   doi:10.1029/2010GL044459.

670   Li J, Wang J (2003) A new North Atlantic Oscillation index and its variability. Adv

671   Atmos Sci 20:661–676

672   Li Y, and Lau NC (2012a) Impact of ENSO in the atmospheric variability over the

673   North Atlantic in late winter—role of transient eddies. J Clim 25:320–342

674   Li Y, and Lau NC (2012b) Contributions of downstream eddy development to the

675   teleconnection between ENSO and the atmospheric circulation over the North

676   Atlantic. J Clim 25:4993–5010

677   Lim EP, Hendon HH, Rashid H (2013) Seasonal predictability of the southern annular

678   mode due to its association with ENSO. J Clim 26:8037–8054

679   Mathieu PP, Sutton RT, Dong BW, Collins M (2004) Predictability of winter climate

680   over the North Atlantic European region during ENSO events. J Clim

681   17:1953–1974

682   Merkel U, Latif M (2002) A high resolution AGCM study of the El Niño impact on

683   the North Atlantic/European sector. Geophys Res Lett 29:1291.

684   doi:10.1029/2001GL013726

685   Moron M, Gouirand I (2003) Seasonal modulation of the ENSO relationship with sea

686   level pressure anomalies over the North Atlantic in October–March 1873–1996.

687   Int J Climatol 23:143–155

688   Neelin JD, Battisti DS, Hirst AC, Jin FF, Wakata Y, Yamagata T, Zebiak SE (1998)

689   ENSO theory. J Geophys Res 103:14 261–14 290

690   Parks TW, Burrus CS (1987) Design of linear-phase finite impulse-response. Digital

691   Filter Design, T. W. Parks and C. S. Burrus, Eds., John Wiley & Sons, 33–110

692   Pozo-Vázquez D, Gamiz-Fortis SR, Tovar-Pescador J, Esteban-Parra MJ, Castro-Diez

693   Y (2005) ENSO events and associated European winter precipitation anomalies.

694   Int J Climatol 25:17–31

695   Quadrelli R, Pavan V, Molteni F (2001) Wintertime variability of Mediterranean

696   precipitation and its links with large-scale circulation anomalies. Clim Dyn

697   17:457–466

Rayner N A, Parker DE, Horton EB, Folland CK, Alexander LV, Rowell DP, Kent EC, Kaplan A (2003) Global analyses of sea surface temperature, sea ice, and night marine air temperature since the late nineteenth century. J Geophys Res 108:4407. doi:10.1029/2002JD002670

Ren HL, Jin FF (2011) Niño indices for two types of ENSO. Geophys Res Lett 38:L04704. doi:10.1029/2010GL046031

Ren HL, Jin FF, Stuecker M, Xie RH (2013), ENSO regime change since the late 1970s as manifested by two types of ENSO. J Meteor Soc Japan 91:835–842

Robertson AW, Mechoso CR, Kim YJ (2000) The influence of the Atlantic sea surface temperature anomalies on the North Atlantic Oscillation. J Clim 13:122–138

Robock A (2000) Volcanic eruptions and climate. Rev Geophys 38:191–219

Rogers JC (1984) The association between the North Atlantic Oscillation and the Southern Oscillation in the Northern Hemisphere. Mon Weather Rev 122:1999–2015

Ropelewski CF, Halpert MS (1987) Global and regional scale precipitation patterns associated with the El Niño/Southern Oscillation. Mon Wea Rev 115:1606–1626

Ropelewski CF, Halpert MS (1996) Quantifying Southern Oscillation-precipitation relationships. J Clim 9:1043–1059

Schopf PS, Suarez MJ (1988) Vacillations in a coupled ocean–atmosphere model. J Atmos Sci 45:549–566

Stuecker M, Jin FF, Timmermann A, McGregor S (2015) Combination Mode Dynamics of the anomalous North-West Pacific Anticyclone. J Clim 28:1093–1111

The GFDL Global Atmospheric Model Development Team (2004) The New GFDL Global Atmosphere and Land Model AM2-LM2: Evaluation with Prescribed SST Simulations. J Clim 17:4641-4673

Toniazzo T, Scaife AA (2006) The influence of ENSO on winter North Atlantic climate. Geophys Res Lett 33:L24704. doi:10.1029/2006GL027881

Trenberth KE, Caron JM (2000) The Southern Oscillation revisited: Sea level pressure, surface temperatures, and precipitation. J Clim 13:4358–4365

728 van Loon H, Madden RA (1981) The Southern Oscillation. Part I: Global associations

729 with pressure and temperature in northern winter. Mon Wea Rev 109:1150–1162

730 Wallace JM, Gutzler DS (1981) Teleconnections in the geopotential field during the

731 Northern Hemisphere winter. Mon Wea Rev 109:784–812

732 Wallace JM, Rasmusson EM, Mitchell TP, Kousky VE, Sarachik ES, Von Storch H

733 (1998) On the structure and evolution of ENSO-related climate variability in the

734 tropical Pacific: Lessons from TOGA. J Geophys Res 103:14 241–14 259

735 Wang B, Wu R, Fu X (2000) Pacific-East Asian teleconnection: How does ENSO

736 affect East Asian Climate? J Clim 13:1517–1536

737 Wang C (2002) Atlantic climate variability and its associated atmospheric circulation

738 cells. J Clim 15:1516–1536

739 Watanabe M, Kimoto M (1999) Tropical–extratropical connection in the Atlantic

740 atmosphere–ocean variability. Geophys Res Lett 26:2247–2250

741 Weng H, Ashok K, Behera SK, Rao SA, Yamagata T (2007) Impacts of recent El Niño

742 Modoki on dry/wet conditions in the Pacific rim during boreal summer. Clim Dyn

743 29:113–129

744 Wilson AB, Bromwich DH, Hines KM (2016) Simulating the mutual forcing of

745 anomalous high-southern latitude atmospheric circulation by El Niño flavors and

746 the Southern Annular Mode. J Clim 29:2291-2309

747 Wilson AB, Bromwich DH, Hines KM, Wang SH (2014) El Niño flavors and their

748 simulated impacts on atmospheric circulation in the high southern latitudes. J

749 Clim 27:8934–8955

750 Wolter K (1987) The Southern Oscillation in surface circulation and climate over the

751 tropical Atlantic, eastern Pacific, and Indian Oceans as captured by cluster

752 analysis. J Clim Appl Meteorol 26:540–558

753 Wu A, Hsieh WW (2004) The nonlinear association between ENSO and the

754 Euro-Atlantic winter sea level pressure. Clim Dyn 23:859–868

755 Wu Z, Zhang P (2015) Interdecadal variability of the mega-ENSO-NAO

756 synchronization in winter. Clim Dyn 45:1117–1128

757 Wyrtki K (1975) El Niño—The dynamic response of the equatorial Pacific Ocean to

758 atmospheric forcing. J Phys Oceanogr 5:572–584

759 Xiao D, Li JP (2011) Mechanism of stratospheric decadal abrupt cooling in the early

760 1990s as influenced by the Pinatubo eruption. Chinese Sci Bull 56:772–780

761 Xie F, Li JP, Tian WS, Feng J, Huo Y (2012) Signals of El Niño Modoki in the

762 tropical tropopause layer and stratosphere. Atmos Chem Phys 12:5295-5237

763 Xie SP, Hu K, Hafner J, Tokinaga H, Du Y, Huang G, Sampe T (2009) Indian Ocean

764 capacitor effect on Indo-Western Pacific climate during the summer following El

765 Niño. J Climate 22:730–747

766 Xie SP, Kosaka Y, Du Y, Hu K, Chowdary JS, Huang G (2016) Indo-Western Pacific

767 Ocean capacitor and coherent climate anomalies in post-ENSO summer: A review.

768 Adv Atmos Sci 33:411–432

769 Yang J, Liu Q, Xie SP, Liu Z, Wu L (2007) Impact of the Indian Ocean SST basin

770 mode on the Asian summer monsoon. Geophys Res Lett 34:L02708.

771 doi:10.1029/2006GL028571

772 Yu JY, Zou Y, Kim ST, Lee T(2012) The changing impact of El Niño on US winter

773 temperature. Geophys. Res. Lett., 39, L15702, doi:10.1029/2012GL052483.

774 Zhang R, Sumi A, Kimoto M (1996) Impacts of El Niño on the East Asian monsoon:

775 A diagnostic study of the ’86/87 and ’91/92 events. J Meteor Soc Japan, 74:49–62

776 Zhang W, Li H, Stuecker M, Jin FF, Turner AG (2016) A new understanding of El

777 Nino's impact over East Asia: Dominance of the ENSO combination mode. J Clim

778 29:4347-4359

779 Zhang W. Wang L, Xiang B, Qi L, He J (2015) Impacts of two types of La Nina on

780 the NAO during boreal winter. Clim Dyn 44:1351-1366

781 Zhang W, Jin FF, Turner A (2014) Increasing autumn drought over southern China

782 associated with ENSO regime shift. Geophys Res Lett 41.

783 doi:10.1002/2014GL060130.

784 Zhang W, Jin FF, Li JP, Ren HL (2011) Contrasting impacts of two-type El Niño over

785 the western North Pacific. J Meteor Soc Japan 89:563–569

786 Zhang W, Jin FF, Zhao JX, Qi L, Ren HL (2013) The possible influence of a

787 non-conventional El Niño on the severe autumn drought of 2009 in Southwest

788   China. J Clim 26:8392–8405

789

Figure Captions

791 Figure 1. (a) Time series of normalized DJF-Niño3.4 (red) and JFM-NAO (blue)

792 indices. (b) Sliding correlation between DJF-Niño3.4 and JFM-NAO indices on

793 with moving windows of 11 (blue) and 21 (red) years. Blue and red dashed

794 horizontal lines in (b) indicate correlation coefficients exceeding the statistical

795 90% confidence level for the 11- and 21- year windows, respectively.

796 Figure 2. Scatterplot of the JFM-NAO index as a function of the normalized

797 DJF-Niño3.4 index for EP El Niño (red dot), CP El Niño (orange dot), EP La Niña

798 (blue dot), and CP La Niña (green dot) events. Stars denote composites of the

799 different type of events, which exceed the statistical 95% confidence level.

800 Figure 3. Composite SST (contour in °C) and near-surface wind (vector in m/s)

801 anomalies during La Niña winters associated with (a) positive NAO phase and (b)

802 negative NAO phase. Light (dark) shading indicates areas for which the SST

803 anomaly composites exceed the 90% (95%) confidence level. The near-surface

804 wind anomalies are shown only when the anomalous wind speed is above 0.5 m/s.

805 Figure 4. Composite SST (contour in °C) and near-surface wind (vector in m/s)

806 anomalies for (a) EP El Niño, (b) CP El Niño, (c) EP La Niña, and (d) CP La Niña.

807 Light (dark) shading indicates the values exceeding the 90% (95%) confidence

808 level. The near-surface wind anomalies below the 80% confidence level are

809 omitted.

810 Figure 5. Composite SLP anomalies (hPa) for (a) EP El Niño, (b) CP El Niño, (c) EP

811 La Niña, and (d) CP La Niña. Horizontal and diagonal lines, and cross-hatched

812 regions indicate where the composites exceed the 80%, 90%, and 95% confidence

813 level, respectively.

814 Figure 6. Meridional-vertical geopotential height anomalies (m) zonally averaged

815 over 10°–80°W in the North Atlantic for (a) EP El Niño, (b) CP El Niño, (c) EP La

816 Niña, and (d) CP La Niña. Shading indicates values exceeding the 80% and 90%

817 confidence level respectively.

818 Figure 7. Composite zonal wind anomalies (m/s) at 300 hPa for (a) EP El Niño, (b)

819 CP El Niño, (c) EP La Niña, and (d) CP La Niña. Light (dark) red and blue

820 　shadings indicate positive and negative anomalies exceeding the 80% (90%)
821 　confidence level, respectively.

822 Figure 8. Composite surface air temperature (℃) for (a) EP El Niño, (b) CP El Niño,
823 　(c) EP La Niña, and (d) CP La Niña. Horizontal and diagonal lines, and
824 　cross-hatched regions indicate where the composites exceed the 80%, 90%, and
825 　95% confidence level, respectively.

826 Figure 9. Ensemble mean JFM SLP response (hPa) to tropical Pacific SST anomaly
827 　forcing of (a) EP El Niño, (b) CP El Niño, (c) EP La Niña, and (d) CP La Niña.
828 　The values of the anomalous NAO indices are given as inserts.

829 Figure 10. Ensemble mean JFM zonal wind anomalies (m/s) at 300 hPa in response to
830 　tropical Pacific SST anomaly forcing of (a) EP El Niño, (b) CP El Niña, (c) EP La
831 　Niña, and (d) CP La Niña.

832 Figure 11. Horizontal distributions of SST (shading in ℃) and SLP (contours in hPa)
833 　anomaly for (a) EP El Niño minus EP La Niña, (b) CP El Niño minus CP La Niña,
834 　(c) EP El Niño plus EP La Niña and (d) CP El Niño plus CP La Niña. Only SST
835 　values exceeding the 95% confidence level are displayed in shading.

836 Figure 12. Same as Figure 12, except that the SLP anomalies (hPa) are the ensemble
837 　mean from the model experiments.

838 Figure 13. Precipitation anomalies (mm/d) over the eastern equatorial Pacific
839 　(155°-90°W, 5°S-5°N) for EP El Niño minus EP La Niña (EPW-EPC), EP El Niño
840 　plus EP La Niña (EPW+EPC), CP El Niño minus CP La Niña (CPW-CPC), and
841 　CP El Niño plus CP La Niña (CPW+CPC).

842 Figure 14. Partial correlation coefficient between the SLP and SST anomalies over the
843 　tropical North Atlantic (0°−30°N, 20°−80°W) after removing the linear Nino3.4
844 　index. The hatching indicates the values exceeding the 95% confidence level.

845 Figure 15. Time-height diagram of zonal wind anomalies (m/s) in NCEP reanalysis
846 　averaged over 10°−80°W at 60°N for (a) EP El Niño, (b) CP El Niño, (c) EP La
847 　Niña and (d) CP La Niña. Shading indicates values exceeding the 90% and 95%
848 　confidence level respectively.

849

850 Table 1. Two types of ENSO years (excluding major tropical volcanic eruption

851 events).

	El Niño	**La Niña**
EP type (8,8)	1951/52, 1952/53, 1963/64, 1965/66, 1969/70, 1972/73, 1976/77, 1997/98	1954/55, 1955/56, 1964/65, 1967/68, 1971/72, 1984/85, 1995/96, 2005/06
CP type (9,8)	1953/54, 1957/58, 1968/69, 1977/78, 1979/80, 1986/87, 2002/03, 2004/05, 2009/10	1973/74, 1974/75, 1975/76, 1988/89, 1998/99, 2000/01, 2010/11, 2011/12

852

853 Table 2. List of the conducted SST perturbation experiments.

Experiment	**Description of the SST perturbation**
EPW	Positive anomalies associated with EP El Niño winters are imposed in the tropical Pacific (30°S–30°N, 120°E–90°W)
CPW	As in EPW but for the CP El Niño winters
EPC	Negative anomalies associated with EP La Niña winters are imposed in the tropical Pacific (30°S–30°N, 120°E–90°W).
CPC	As in EPC but for the CP La Niña winters

854

855 Table 3. Linear correlation coefficients (R) between DJF-Niño3.4 and JFM-NAO

856 indices (with sample size n) for different episodes. Asterisks indicate correlation

857 coefficients exceeding the 95% confidence level.

	All years	All years except volcano years	All years except volcano and EP La Niña years	El Niño and CP La Niña years	All years except volcano and ENSO years
n	61	55	47	25	22
R	-0.23	-0.33*	-0.50*	-0.63*	-0.04

858

859

860

864

868
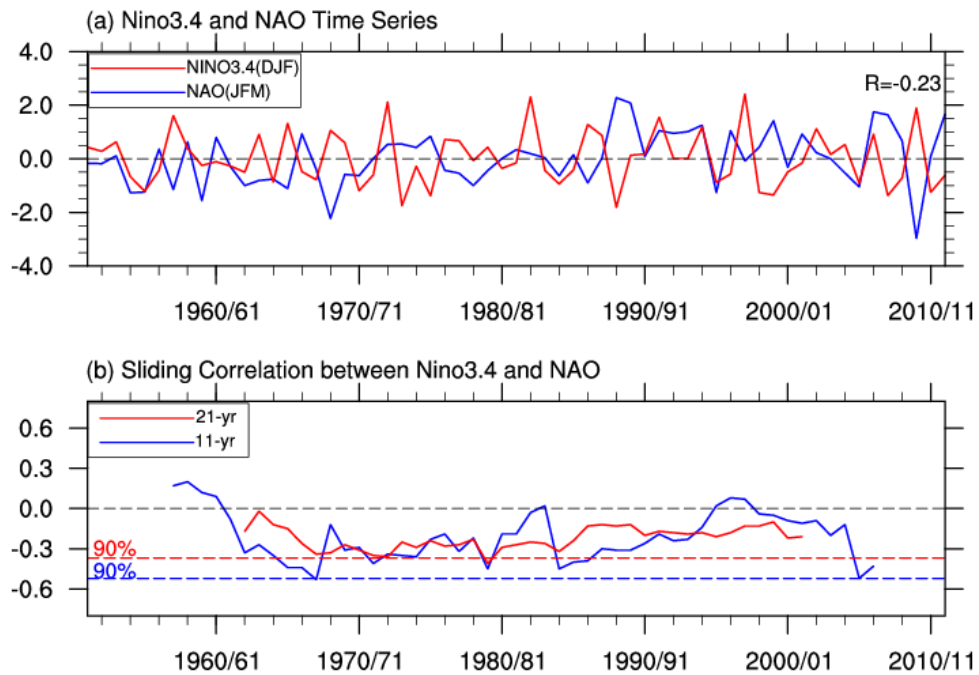
Figure 1. (a) Time series of normalized DJF-Niño3.4 (red) and JFM-NAO (blue)

indices. (b) Sliding correlation between DJF-Niño3.4 and JFM-NAO indices on with

moving windows of 11 (blue) and 21 (red) years. Blue and red dashed horizontal lines

in (b) indicate correlation coefficients exceeding the statistical 90% confidence level

for the 11- and 21- year windows, respectively.

874

875

878
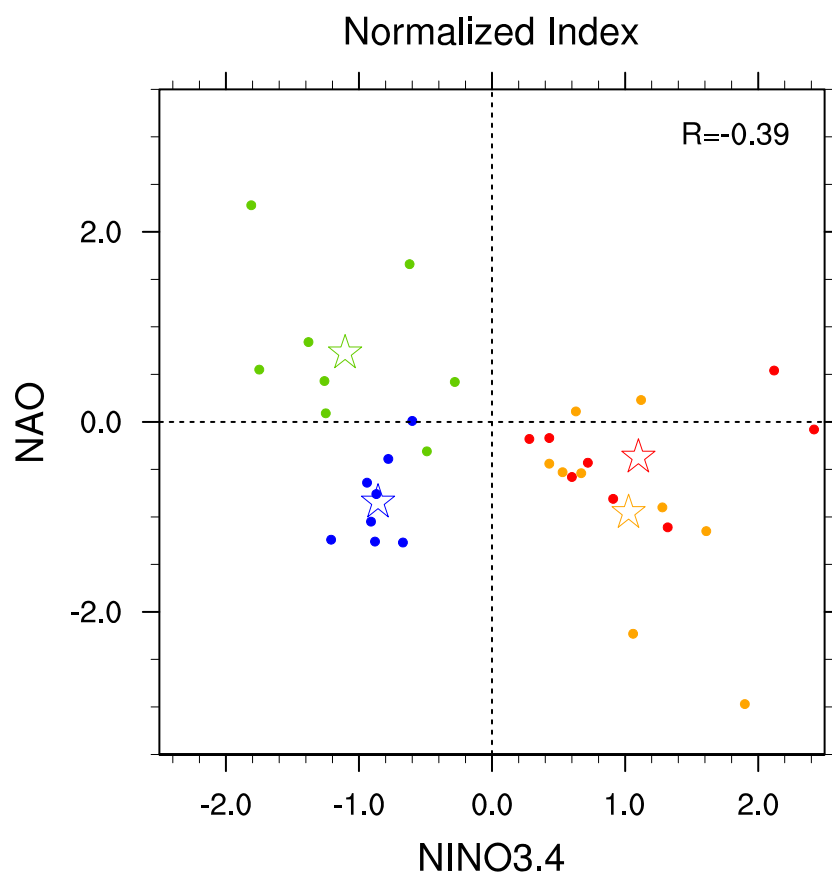
Figure 2. Scatterplot of the JFM-NAO index as a function of the normalized DJF-Niño3.4 index for EP El Niño (red dot), CP El Niño (orange dot), EP La Niña (blue dot), and CP La Niña (green dot) events. Stars denote composites of the different type of events, which exceed the statistical 95% confidence level.

900

901

902

903

904

905

906

907

908

909

910
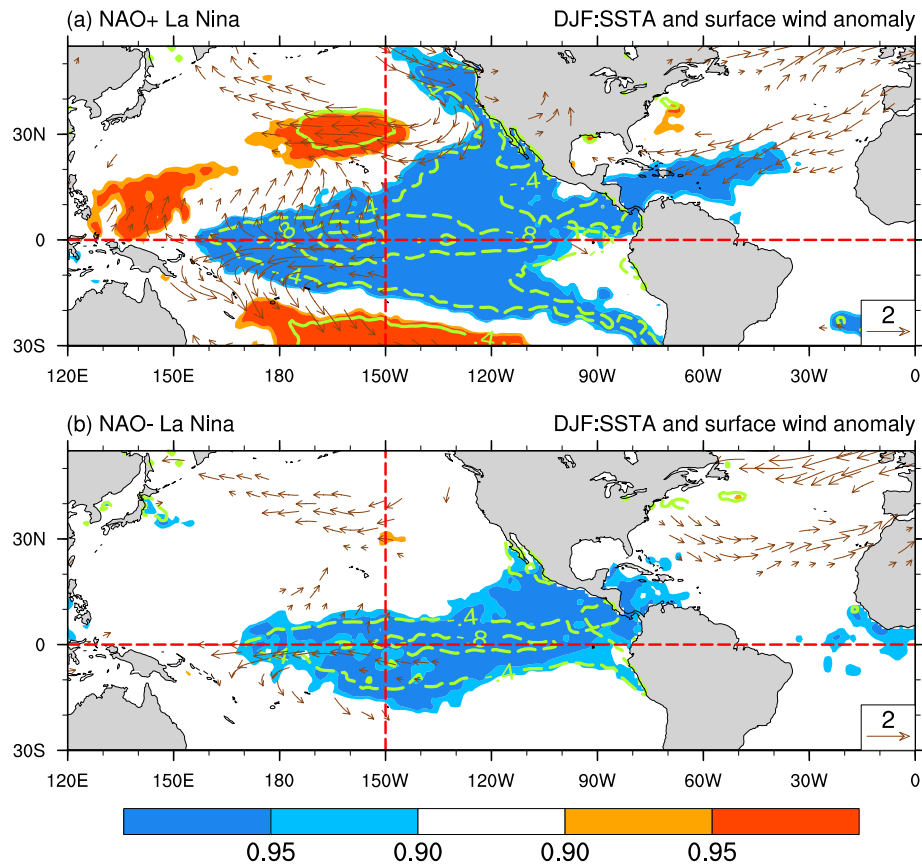
Figure 3. Composite SST and near-surface wind anomalies (°C) during La Niña

winters associated with (a) positive NAO phase and (b) negative NAO phase. Light

(dark) shading indicates areas for which the SST anomaly composites exceed the 90%

(95%) confidence level. The near-surface wind anomalies are shown only when the

anomalous wind speed is above 0.5 m/s.

916

917

918

919
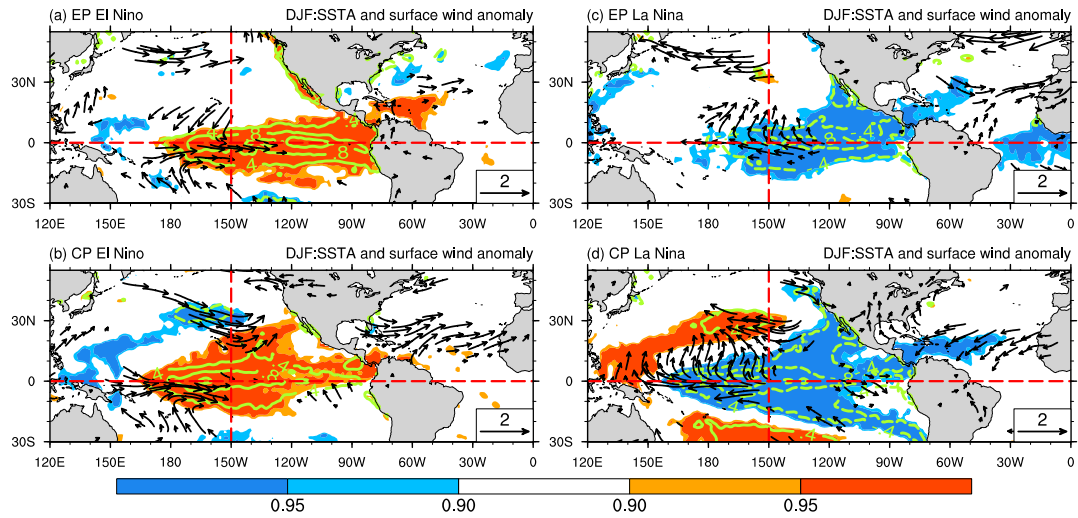
Figure 4. Composite SST (contour in °C) and near-surface wind (vector in m/s) anomalies for (a) EP El Niño, (b) CP El Niño, (c) EP La Niña, and (d) CP La Niña. Light (dark) shading indicates the values exceeding the 90% (95%) confidence level. The near-surface wind anomalies below the 80% confidence level are omitted.
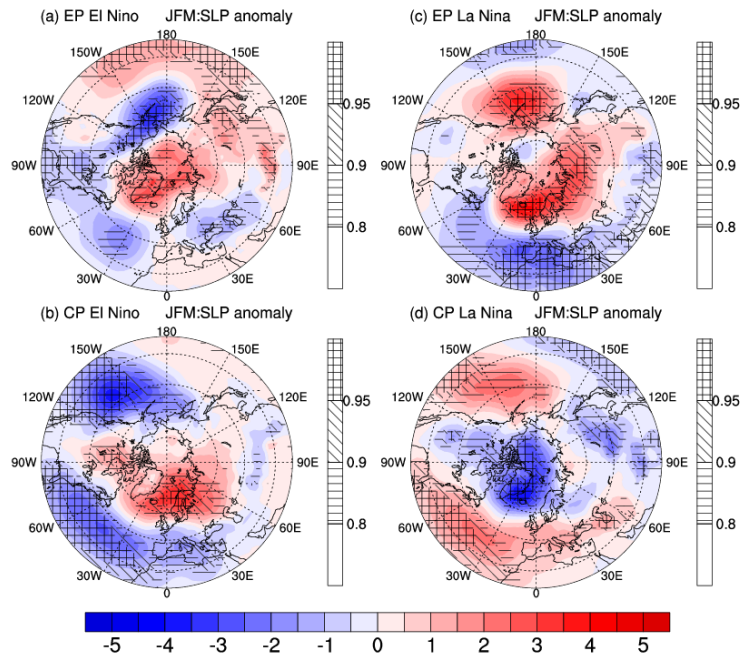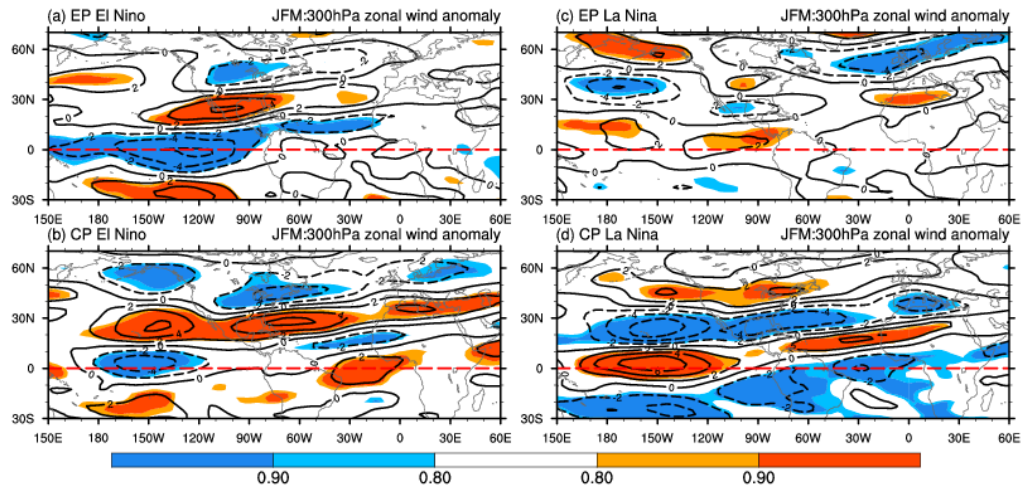
43

931

932

Figure 5. Composite SLP anomalies (hPa) for (a) EP El Niño, (b) CP El Niño, (c) EP La Niña, and (d) CP La Niña. Horizontal and diagonal lines, and cross-hatched regions indicate where the composites exceed the 80%, 90%, and 95% confidence level, respectively.

945

946

947

948

949
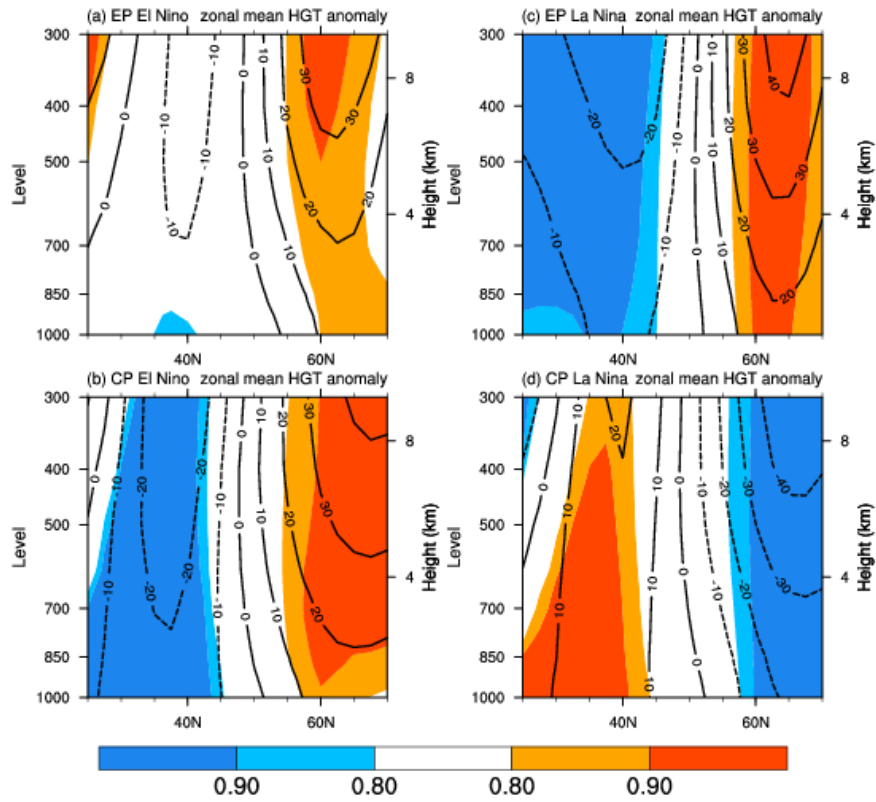
Figure 6. Meridional-vertical geopotential height anomalies (m) zonally averaged over 10°–80°W in the North Atlantic for (a) EP El Niño, (b) CP El Niño, (c) EP La Niña, and (d) CP La Niña. Shading indicates values exceeding the 80% and 90% confidence level respectively.

965

966

967

968

Figure 7. Composite zonal wind anomalies (m/s) at 300 hPa for (a) EP El Niño, (b) CP El Niño, (c) EP La Niña, and (d) CP La Niña. Light (dark) red and blue shadings indicate positive and negative anomalies exceeding the 80% (90%) confidence level, respectively.
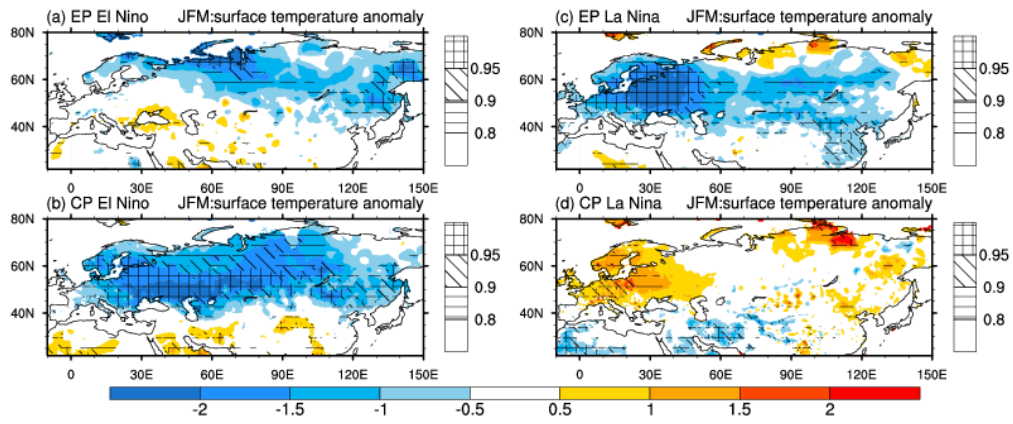
983
984

985

986

987

988

989

990

991

Figure 8. Composite surface air temperature (℃) for (a) EP El Niño, (b) CP El Niño, (c) EP La Niña, and (d) CP La Niña. Horizontal and diagonal lines, and cross-hatched regions indicate where the composites exceed the 80%, 90%, and 95% confidence level, respectively.

996

997

998

999

1000

1001

1002

1003

1004

1005
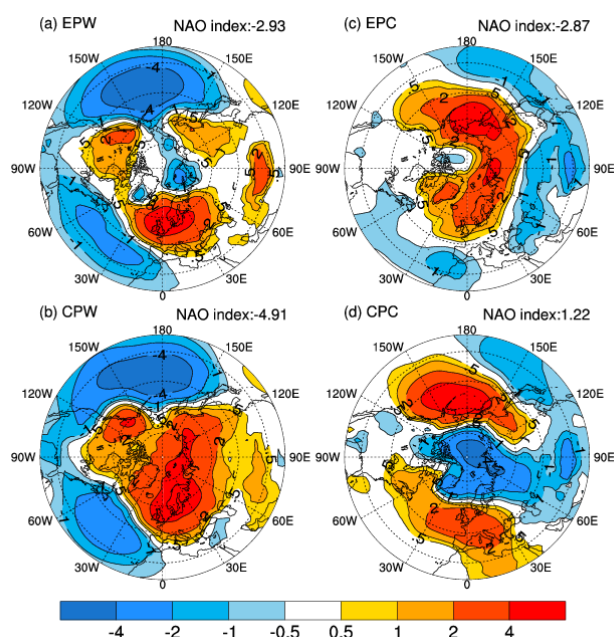
Figure 9. Ensemble mean JFM SLP response (hPa) to tropical Pacific SST anomaly

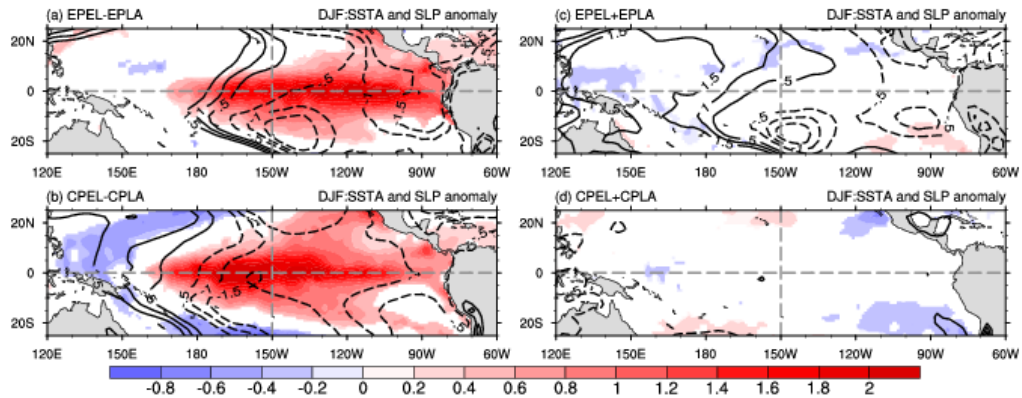forcing of (a) EP El Niño, (b) CP El Niño, (c) EP La Niña, and (d) CP La Niña. The

values of the anomalous NAO indices are given as inserts.

1009

1010

1011

1012

1013

1014

1015

1016

1017
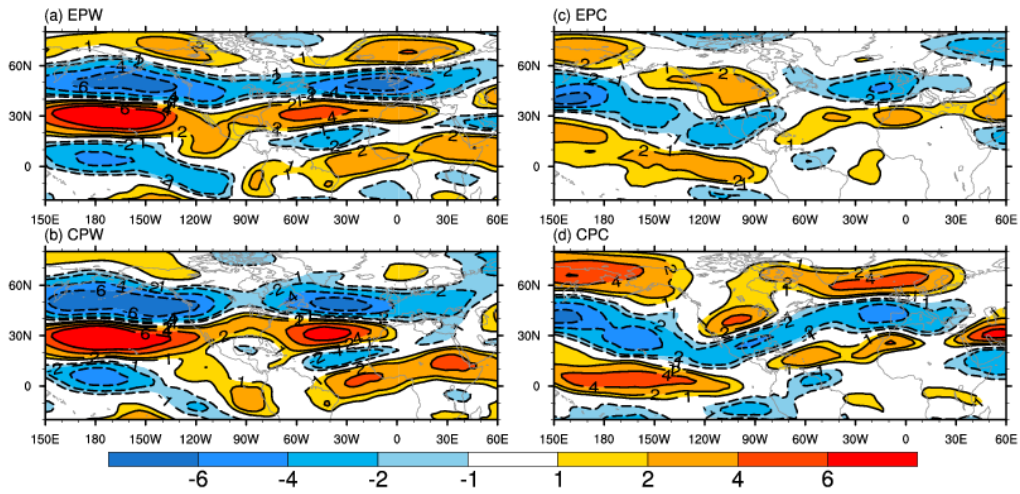
1018 Figure 10. Ensemble mean JFM zonal wind anomalies (m/s) at 300 hPa in response to

1019 tropical Pacific SST anomaly forcing of (a) EP El Niño, (b) CP El Niña, (c) EP La

1020 Niña, and (d) CP La Niña.

1021

1022

1023

1024

1025

1026

1027

1028

1029

1030 Figure 11. Horizontal distributions of SST (shading in ℃) and SLP (contours in hPa)

1031 anomaly for (a) EP El Niño minus EP La Niña, (b) CP El Niño minus CP La Niña, (c)

1032 EP El Niño plus EP La Niña and (d) CP El Niño plus CP La Niña. Only SST values

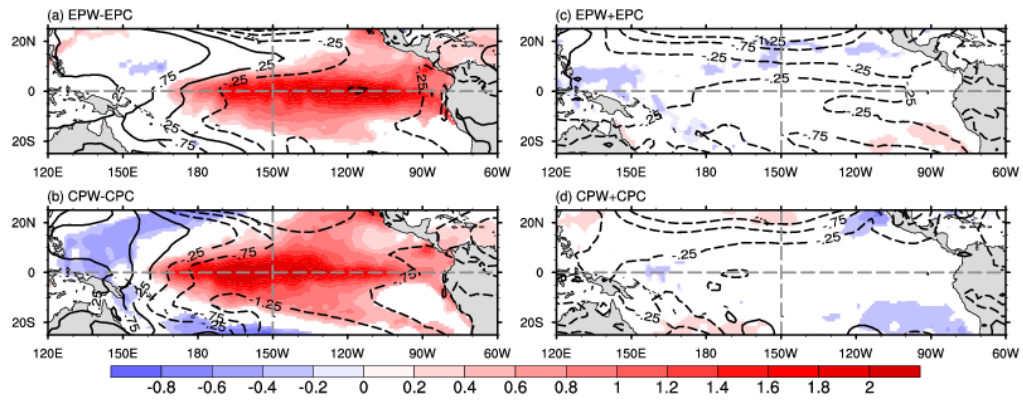1033 exceeding the 95% confidence level are displayed in shading.

1034

1035

1036

1037

1038

1039

1040

1041

1042

1043   Figure 12. Same as Figure 12, except that the SLP anomalies (hPa) are the ensemble

1044   mean from the model experiments.

1045

1046

1047

1048

1049

1050

1051

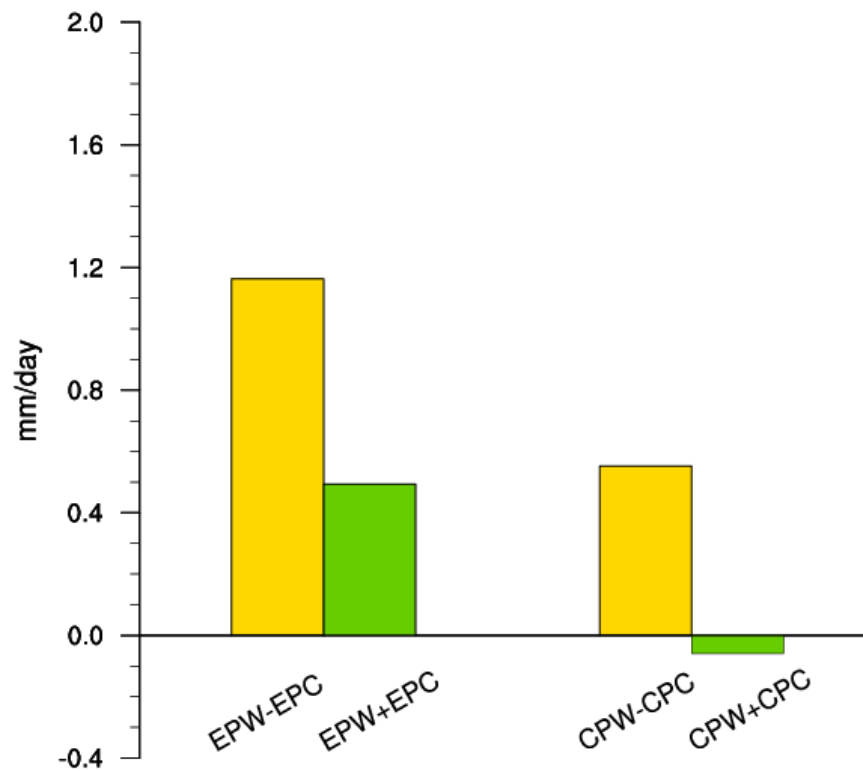1052

1053

1054

1055

1056

1057

1058
1059

Figure 13. Precipitation anomalies (mm/d) over the eastern equatorial Pacific (155°-90°W, 5°S-5°N) for EP El Niño minus EP La Niña (EPW-EPC), EP El Niño plus EP La Niña (EPW+EPC), CP El Niño minus CP La Niña (CPW-CPC), and CP El Niño plus CP La Niña (CPW+CPC).
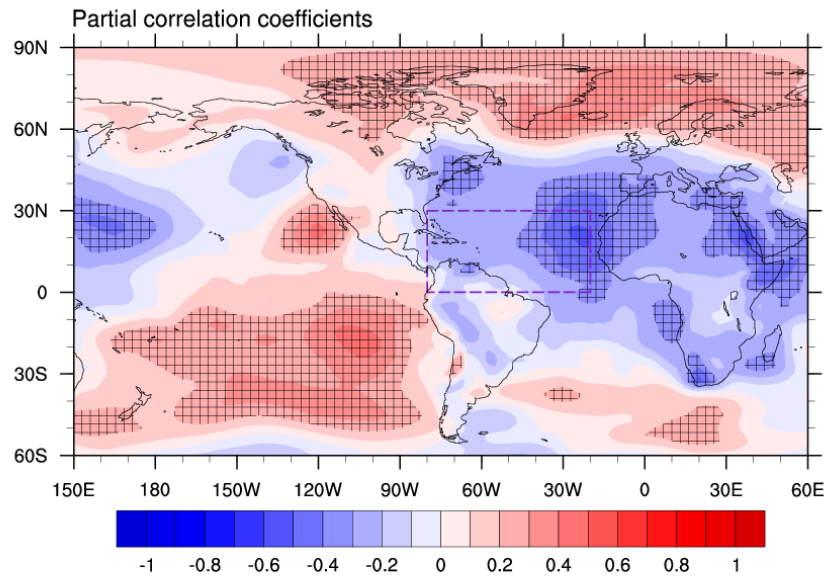
1064

1065

1066

Figure 14. Partial correlation coefficient between the SLP and SST anomalies over the

tropical North Atlantic (0°–30°N, 20°–80°W) after removing the linear Nino3.4 index.

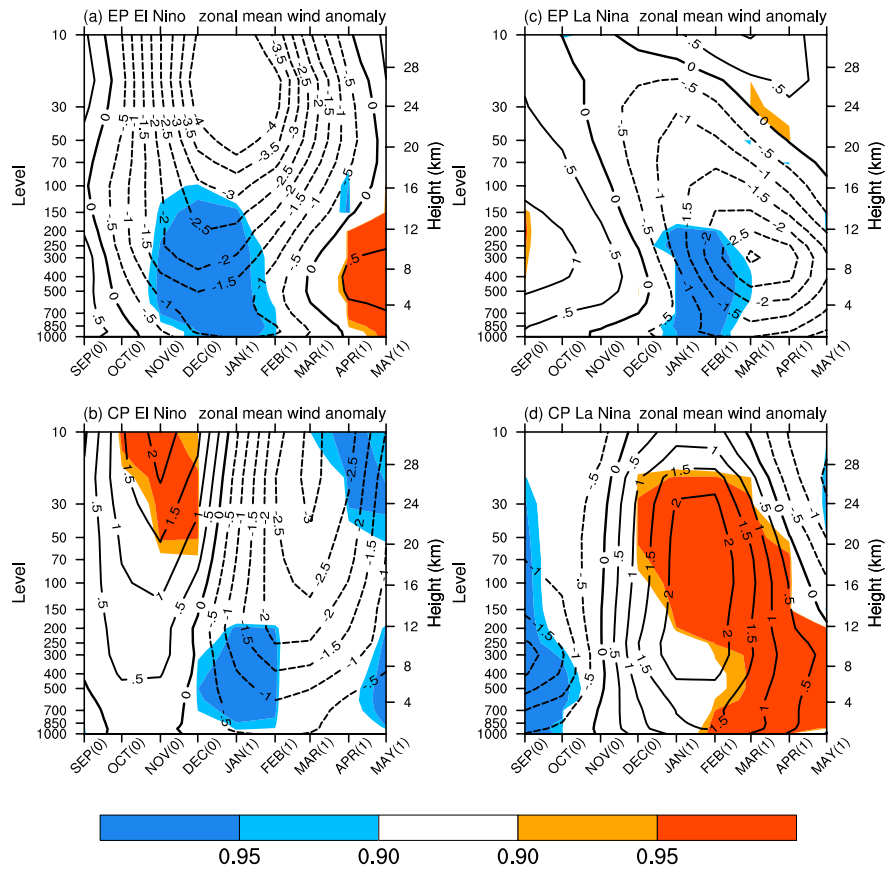The hatching indicates the values exceeding the 95% confidence level.

1078

1092 Figure 15. Time-height diagram of zonal wind anomalies (m/s) in NCEP reanalysis

1093 averaged over 10°−80°W at 60°N for (a) EP El Niño, (b) CP El Niño, (c) EP La Niña

1094 and (d) CP La Niña. Shading indicates values exceeding the 90% and 95% confidence

1095 level respectively.